PLOS | GENETICS

RESEARCH ARTICLE

Network Analysis of Genome-Wide Selective Constraint Reveals a Gene Network Active in Early Fetal Brain Intolerant of Mutation

Jinmyung Choi[1], Parisa Shooshtari[1], Kaitlin E. Samocha[2,3,4,5], Mark J. Daly[2,3,4], Chris Cotsapas[1,2,3,4,6]*

1 Department of Neurology, Yale School of Medicine, New Haven Connecticut, United States of America, **2** Analytic and Translational Genetics Unit, Department of Medicine, Massachusetts General Hospital and Harvard Medical School, Boston, Massachusetts, United States of America, **3** Program in Medical and Population Genetics, Broad Institute of Harvard and MIT, Cambridge, Massachusetts, United States of America, **4** Stanley Center for Psychiatric Research, Broad Institute of Harvard and MIT, Cambridge, Massachusetts, United States of America, **5** Program in Genetics and Genomics, Biological and Biomedical Sciences, Harvard Medical School, Boston, Massachusetts, United States of America, **6** Department of Genetics, Yale School of Medicine, New Haven CT, United States of America

* cotsapas@broadinstitute.org

OPEN ACCESS

Citation: Choi J, Shooshtari P, Samocha KE, Daly MJ, Cotsapas C (2016) Network Analysis of Genome-Wide Selective Constraint Reveals a Gene Network Active in Early Fetal Brain Intolerant of Mutation. PLoS Genet 12(6): e1006121. doi:10.1371/journal.pgen.1006121

Editor: Greg Gibson, Georgia Institute of Technology, UNITED STATES

Received: January 19, 2016

Accepted: May 20, 2016

Published: June 15, 2016

Data Availability Statement: All relevant data are within the paper and its Supporting Information files.

Funding: The authors received no specific funding for this work.

Competing Interests: The authors have declared that no competing interests exist.

Abstract

Using robust, integrated analysis of multiple genomic datasets, we show that genes depleted for non-synonymous *de novo* mutations form a subnetwork of 72 members under strong selective constraint. We further show this subnetwork is preferentially expressed in the early development of the human hippocampus and is enriched for genes mutated in neurological Mendelian disorders. We thus conclude that carefully orchestrated developmental processes are under strong constraint in early brain development, and perturbations caused by mutation have adverse outcomes subject to strong purifying selection. Our findings demonstrate that selective forces can act on groups of genes involved in the same process, supporting the notion that purifying selection can act coordinately on multiple genes. Our approach provides a statistically robust, interpretable way to identify the tissues and developmental times where groups of disease genes are active.

Author Summary

Some genes are extremely intolerant of mutations that alter their amino acid sequence. Such mutations are highly likely to drive disease, and previous reports have implicated these genes in multiple diseases. To better understand the function of these constrained genes and their place in cellular organization, we developed a framework to ask if these genes form biochemical networks expressed in specific tissues and developmental timepoints. Using clustering analysis over protein-protein interaction maps, we show that 72/107 such genes form a densely connected network. Using another new method, we found that these 72 genes are coordinately expressed in fetal brain and early blood cell precursors, but not other tissues, in the Roadmap Epigenomic Project, and then show that this

gene module is active in very early developmental time points of the hippocampus included in the Brainspan Atlas. We also show that these genes, when mutated, tend to cause genetic diseases. Thus we demonstrate that evolution constrains mutation of key mechanisms that must therefore require careful control in both time and space for development to occur normally.

Introduction

Genetic variation is introduced into the human genome by spontaneously arising *de novo* mutations in the germline. The majority of these mutations have, at most, modest effects on phenotype; they are thus subject to nearly neutral drift and can be transmitted through the population, with some increasing in frequency to become common variants. Conversely, *de novo* mutations with large effects on phenotype may be subject to many different selective forces, both positive and negative, with the latter resulting in either the variant being completely lost from the population or maintained at very low frequencies [1].

Large-scale DNA sequencing can now be used to comprehensively assess *de novo* mutations, with many current applications focusing on the protein-coding portion of the genome (the exome). This approach has been used to identify causal genes and variants in rare Mendelian diseases: for example, exome sequencing of ten affected individuals with Kabuki syndrome identified the methyl transferase *KMT2D* (formerly *MLL2*) as causal, after substantial *post hoc* data filtering [2]. In complex traits, this approach has successfully identified pathogenic genes harboring *de novo* mutations in autism spectrum disorders [3], intellectual disability [4] and two epileptic encephalopathies [5]; notably, all these studies sequenced the exomes of parent-affected offspring trios and quantified the background rate of *de novo* mutations in each gene using formal analytical approaches. They were thus able to identify genes harboring a statistically significant number of mutations, which are likely to be causal for disease [5,6].

These large-scale exome sequencing studies have demonstrated that the rate of non-synonymous *de novo* mutations is markedly depleted in some genes, and that these genes are more likely to harbor disease-causing mutations [6]. As synonymous *de novo* mutations occur at expected frequencies, this depletion is not driven by variation in the local overall mutation rate; instead, these genes appear to be intolerant of changes to amino acid sequence and are thus under selective constraint, with non-synonymous mutations removed by purifying selection. These genes represent a limited number of fundamental biological roles, which suggests that entire processes, rather than single genes, are under selective constraint. This is consistent with the extreme polygenicity of most human traits, where hundreds of genes play a causal role in determining organismal phenotype [7,8]. These genes must participate in the same cellular processes, but uncovering the relevant connections and the cell populations and developmental stages in which they occur remains a challenge. We and others have described statistical frameworks to test connectivity within a nominated set of genes [9–11] by considering how genes interact either in annotated pathways or in networks derived from protein interactions or gene co-expression across tissues, and these approaches have been successfully applied to detecting networks of genes underlying neurodevelopmental disease [12]. These studies have demonstrated that genes underlying complex diseases tend to aggregate in networks; we hypothesize that the same is true of constrained genes. However, unlike disease traits where the relevant organ system is known and hypotheses about pathogenesis can by formulated, the phenotypic targets of selective forces are usually unknown. Thus, systematic genome-wide approaches to assessing connectivity between a set of genes of interest and to identify relevant tissues are

required to investigate how selective constraint acts on groups of genes and uncover the relevant physiology.

To address these issues we have developed a robust, unbiased framework and applied it to genome-wide selective constraint data derived from exome sequences of 6,503 individuals [6]. We identified a single, statistically significant subnetwork of 72 interacting genes highly intolerant of non-synonymous variation, with no other interacting groups of genes showing evidence of such coordinate constraint. To establish biological context for this subnetwork, we developed a robust approach to test for preferential expression of the module as a whole, rather than the individual constituent genes. Using gene expression data from the cosmopolitan atlas of tissues in the Roadmap Epigenome Project [13,14], we found that this subnetwork is preferentially expressed in several early-stage tissues, with the strongest enrichment in fetal brain. To more carefully dissect the role of this subnetwork in the central nervous system, we analyzed expression data from BrainSpan [15], an atlas of the developing human brain, and found that the constrained gene subnetwork is preferentially expressed in the early development of the hippocampus. Consistent with this observation, this module is enriched for genes mutated in neurological, but not other, Mendelian disorders. We thus show that selective constraint acts on a set of interacting genes active in early brain development, and that these genes are in fact intolerant of mutation. Our **P**rotein **I**nteraction **N**etwork **T**issue **S**earch (PINTS) framework is publicly available at https://github.com/cotsapaslab/PINTSv1.

Results

Calculating selective constraint scores

We have previously described a framework to assess selective constraint across coding sequences in the genome [6]. Briefly, we calibrated an expectation for all possible conversions of one base to another by mutation from non-coding sequence. For each transition, we modeled the effect of the surrounding sequence and its conservation across species to correct for context effects. We then counted the number of synonymous and non-synonymous variants in the coding sequence of each gene in the genome and derived a statistic of constraint on each class of variation compared to this global expectation. We found that a number of genes show decreased rates of non-synonymous substitution but expected rates of synonymous substitution, consistent with purifying selection removing the non-synonymous alleles from the population.

Analysis framework description

If constrained genes lie in biologically meaningful networks, we expect them to (i) interact and (ii) be expressed in the same tissues. We developed a robust, modular workflow (**PINTS**–**P**rotein **I**nteraction **N**etwork **T**issue **S**earch; Fig 1) to test both of these hypotheses at a genome-wide level. To detect interactions between constrained genes we used a high-confidence protein-protein interaction network (InWeb [16]), and employed a clustering algorithm previously validated on such networks [17]. We assessed significance empirically by randomly reassigning constraint scores to genes (see Materials and Methods and S1 Text). We then tested any significant subnetworks for preferential expression in the diverse tissue atlas provided by the Roadmap Epigenome Project (REP), which assays gene expression in 27 human primary samples across the developmental spectrum [14]. Our final dataset is comprised of 9729 genes both present in InWeb and detected in at least one REP tissue.

Our workflow is both modular and flexible: clustering algorithms, gene-gene relationships and tissue atlases can be replaced as required, so that analyses can be tailored to suit specific

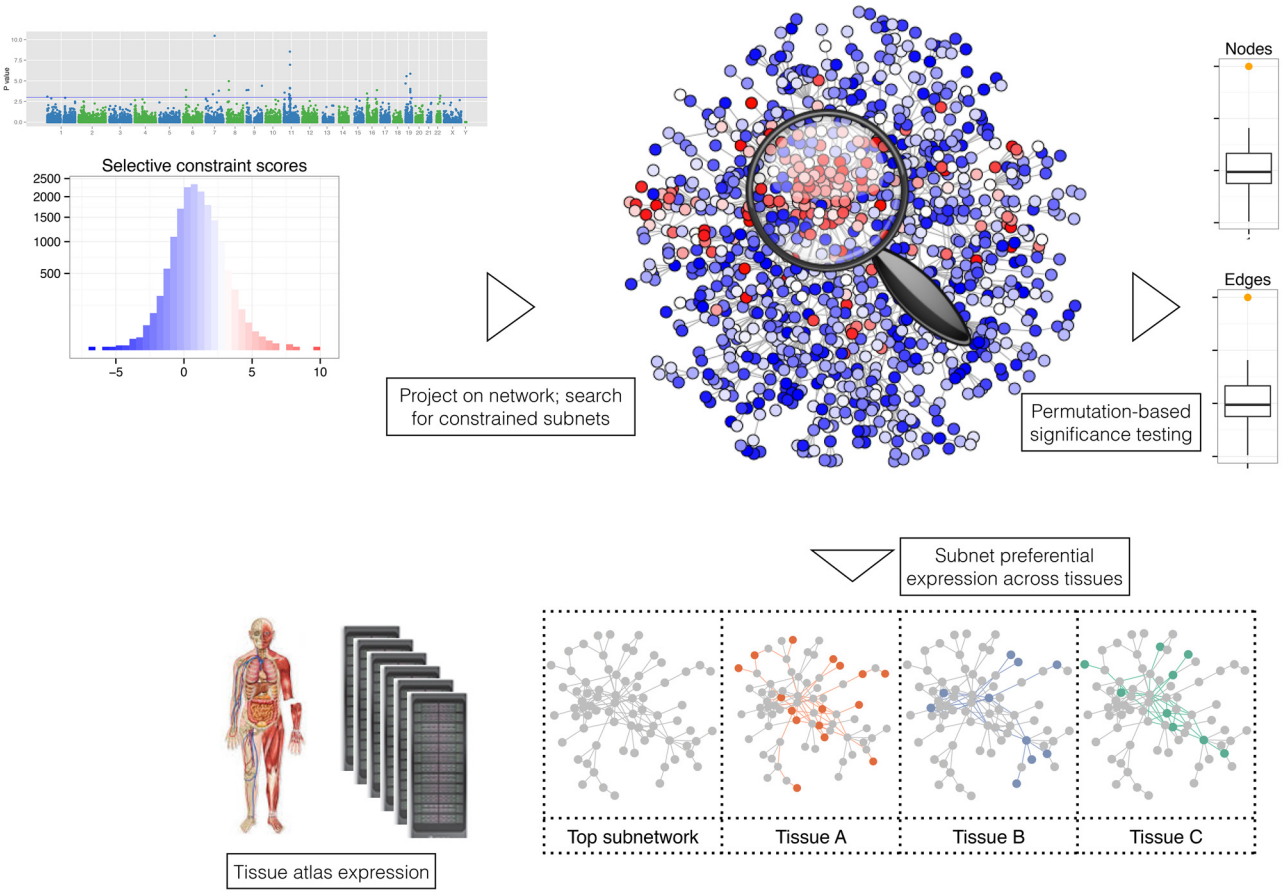

Fig 1. the Protein Interaction Network Tissue Search (PINTS) workflow. We project gene-wise selective constraint scores [6] onto the InWeb protein-protein interaction dataset [16] and use a heuristic version of the prize-collecting Steiner Tree algorithm [17,29] to detect clusters of interacting constrained genes. We assess significance empirically, by randomly assigning the scores to genes 1000 times and calibrating detected subnetwork parameters. We then test any significant subnetwork for usual patterns of preferential expression [32] across the Roadmap Epigenome Project expression data [14], a cosmopolitan tissue atlas, using a Markov random field approach. The approach is flexible and modular, so gene interaction and tissue expression reference datasets can be altered according to the application.

doi:10.1371/journal.pgen.1006121.g001

biological problems. A flexible implementation, including all data described here, is freely available as an R package at https://github.com/cotsapaslab/PINTSv1.

Highly constrained genes form a protein interaction module expressed in fetal tissues and the immune system

We define highly constrained genes as those with evidence of constraint on non-synonymous *de novo* substitutions ($p < 5 \times 10^{-6}$, Bonferroni correction for the number of genes in our InWeb dataset) but null synonymous constraint scores, indicating intolerance to functionally relevant mutation rather than fluctuations in the local mutation rate [6]. Of these, 107/9729 genes pass this stringent threshold (binomial $p < 2.2 \times 10^{-16}$; S1 Table), and form the core of the analysis presented here. We found that 67/107 form a connected subnetwork (Fig 2A; Table 1). Five additional genes are included as our cluster detection algorithm by design looks for a backbone of null nodes connected to many signal nodes. To assess the significance of this observation, we randomly distribute constraint scores to InWeb nodes 1000 times and find that the constrained subnetwork is larger (number of nodes: $p < 0.001$) and more densely

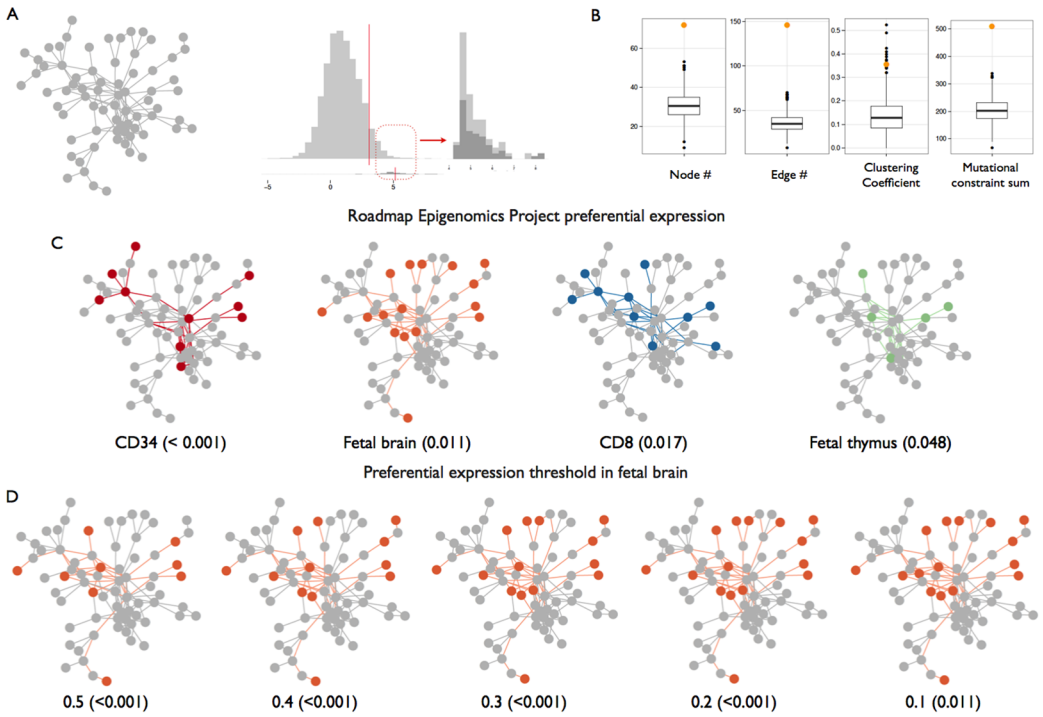

Fig 2. selectively constrained genes form a 72-member network, preferentially expressed in fetal brain, heart and immune cell populations. A: constrained genes form a connected subnetwork of genes in the extreme of the constraint score distribution. B: the constrained subnetwork contains more genes (node $p < 0.001$), has more connections (edge $p < 0.001$), is more densely connected (clustering coefficient $p = 0.008$) and explains more total constraint (sum $p < 0.001$) than expected by chance (orange dots) compared to networks discovered in 1000 permutations of the constraint data (boxplots and black dots). C: the constrained subnetwork is preferentially expressed in a subset of Roadmap Epigenome Project tissues, including fetal brain. Preferentially expressed nodes and the shortest paths connecting them are in color; grey nodes are not preferentially expressed in each displayed tissue. D: The most consistent preferential expression signal is seen in fetal brain, which is robust to stringency of preferential expression threshold.

doi:10.1371/journal.pgen.1006121.g002

connected (number of edges: $p < 0.001$; clustering coefficient: $p = 0.008$) than expected by chance (Fig 2B). As such, it also explains more total constraint in the genome than expected (sum of constraint scores: $p < 0.001$). After accounting for the genes forming this subnetwork, we found no evidence that the remaining 35 genes form statistically significant subnetworks by our criteria.

The genes in the constrained subnetwork appear to represent several fundamental cell processes, most notably mitosis and cell proliferation (*SMC1A*, *SMC3*, *CTNNB1*) and transcriptional regulation (*CHD3*, *CHD4*, *SMARCA4*). We performed a formal pathway analysis to further test this and found enrichment of several annotated pathways reflecting these fundamental processes (Table 2). Encouraged that our detected subnetwork represents one or more biological processes under constraint, we sought to add cellular context to our observations. In particular, we wanted to determine if this group of genes is preferentially expressed in particular tissues, indicating a likely site of action. We thus developed an approach to estimate the joint probability of preferential expression of the genes in the subnetwork in each tissue of an atlas of expression data, while accounting for how frequently each gene is detected across the entire atlas. We applied our approach, which uses Markov random fields, to the expression data on 27 primary tissues and cell lines available from the Roadmap Epigenome Project. Using two conservative permutation-based significance tests, we find the constrained

Table 1. A 72-member constrained gene subnetwork. We find that 67/107 significantly constrained genes form a single protein-protein interaction subnetwork. Five additional genes are also included (gray shading), as our cluster detection algorithm by design looks for a backbone of null nodes connected to many signal nodes. As shown in Fig 2, the subnetwork is significantly larger and more densely connected than expected by chance, and is preferentially expressed in a subset of early-stage neural and immune tissues.

Gene	Constraint score	Chr	Start	End	Gene	Constraint score	Chr	Start	End
DYNC1H1	9.977	14	101964528	102050792	*UBR4*	4.940	1	19074506	19210276
PRPF8	8.302	17	1650629	1684882	*CHD3*	4.905	17	7884806	7912760
HUWE1	7.973	X	53532096	53686729	*USP7*	4.866	16	8892094	8964514
SMARCA4	6.604	19	10961001	11065395	*PRPF6*	4.826	20	63981135	64033100
POLR2A	6.578	17	7484366	7514618	*GNAS*	4.806	20	58839718	58911192
RYR2	6.436	1	237042205	237833988	*THOC2*	4.791	X	123600561	123733056
MED12	6.388	X	71118556	71142454	*FRY*	4.772	13	32031300	32299122
SNRNP200	6.166	2	96274336	96305515	*OGT*	4.753	X	71533083	71575897
CHD4	6.162	12	6570083	6607476	*POLR2B*	4.729	4	56977722	57031168
MTOR	5.974	1	11106535	11262507	*KCNMA1*	4.687	10	76869601	77638595
GRIN1	5.971	9	137138390	137168762	*TAOK1*	4.685	17	29390464	29551904
PPFIA3	5.794	19	49119389	49151026	*BRWD3*	4.683	X	80670854	80809688
MLL	5.747	11	118436490	118526832	*SPTAN1*	4.671	9	128552558	128633665
UBR5	5.720	8	102253012	102412841	*PHIP*	4.670	6	78935867	79078236
ITPR1	5.589	3	4493348	4847840	*DDB1*	4.670	11	61299451	61342596
CLTC	5.547	17	59619689	59696956	*HSPA2*	4.665	14	64535905	64546173
FLNA	5.541	X	154348524	154374638	*SPEG*	4.644	2	219434846	219498287
UPF1	5.514	19	18831938	18868236	*SMC3*	4.639	10	110567691	110604636
HCFC1	5.450	X	153947553	153971807	*MYH10*	4.629	17	8474205	8630761
DHX30	5.428	3	47802909	47850195	*XPO1*	4.621	2	61477849	61538626
SPTBN1	5.423	2	54456285	54671445	*CUL3*	4.610	2	224470150	224585397
SF3B1	5.418	2	197389784	197435091	*IRS2*	4.592	13	109752698	109786568
SMARCA2	5.387	9	2015219	2193624	*ADCY1*	4.587	7	45574140	45723116
CACNA1I	5.363	22	39570753	39689737	*APC2*	4.564	19	1446302	1473244
SMC1A	5.360	X	53374149	53422728	*ZBTB17*	4.547	1	15941869	15976132
GRIN2B	5.334	12	13537337	13980119	*TLN1*	4.517	9	35696948	35732395
GRIN2D	5.211	19	48394875	48444931	*MYH9*	4.496	22	36281281	36388018
TAF1	5.178	X	71366239	71532374	*EEF2*	4.478	19	3976056	3985469
VCP	5.162	9	35056064	35073249	*PDS5A*	4.451	4	39822863	39977956
CNOT1	5.146	16	58519951	58629886	*PRKD2*	4.438	19	46674275	46717127
TRIO	5.109	5	14143702	14532128	*BRD4*	4.436	19	15235519	15332545
CYFIP2	5.100	5	157266079	157395598	*HSPA8*	4.364	11	123057489	123063230
SUPT5H	5.065	19	39436156	39476670	*CTNNB1*	4.198	3	41194837	41260096
FZD8	5.028	10	35638249	35642278	*UBC*	3.997	12	124911604	124917368
TNPO2	4.993	19	12699194	12724011	*PIK3CD*	3.858	1	9651732	9729114
GTF2I	4.945	7	74657667	74760692	*PIK3R1*	2.170	5	68215720	68301821

doi:10.1371/journal.pgen.1006121.t001

subnetwork is preferentially expressed in a number of fetal and immune tissues (Fig 2C and Table 3), including fetal brain (permuted $p < 0.001$), the immune cell subpopulations marked by CD34 (permuted $p < 0.001$) and CD8 (permuted $p = 0.017$) and fetal thymus (permuted $p = 0.048$). We note that, whilst only a subset of genes are expressed in any one tissue, the combinations of genes expressed in these tissues is highly statistically significant: each gene is only expressed in a small subset of the tissues interrogated, so the cumulative probability of seeing these genes coordinately expressed in any one tissue is small.

Table 2. The 72-member constrained gene subnetwork is enriched for canonical pathways reflecting neuronal and immune functionality and basic aspects of cell cycle control. We tested pathways from two sources (the Reactome database and KEGG, the Kyoto Encyclopedia of Genes and Genomes), assessing how many genes are in each pathway (All), how many map onto the 9729 inteconnected genes in our analysis (Mapped), and how many are present in the constrained subnetwork (Subnetwork). We assess significance using both the GSEA approach of a Kolmogorov-Smirnov (KS) test and a simple hypergeometric (HG) test of expected overlaps.

Name	All	Mapped	Subnetwork	KS	HG
Developmental biology (Reactome)	397	344	10	2.53E-19	1.83E-05
Immune system (Reactome)	934	702	9	4.98E-08	1.96E-02
Adaptive immune system (Reactome)	540	421	8	3.13E-10	2.08E-03
Axon guidance (Reactome)	252	220	8	4.62E-16	1.65E-05
mRNA Processing (Reactome)	162	120	8	9.06E-12	1.05E-07
Calcium signaling pathway (KEGG)	179	163	7	6.00E-08	1.36E-05
Spliceosome (KEGG)	129	85	7	5.32E-21	9.60E-08
mRNA splicing (Reactome)	112	74	7	6.26E-20	3.19E-08
Processing of capped intron containing pre-mRNA (Reactome)	141	102	7	3.21E-13	3.99E-07
Pathways in cancer (KEGG)	329	301	6	4.05E-12	4.21E-03
Regulation of actin cytoskeleton (KEGG)	217	188	6	8.08E-13	2.74E-04
Cell cycle (Reactome)	422	332	6	7.95E-03	7.12E-03
mRNA splicing minor pathway (Reactome)	46	20	6	2.90E-05	3.56E-11
Signalling by NGF (Reactome)	218	191	6	3.04E-21	3.02E-04
Focal adhesion (KEGG)	202	188	5	9.72E-07	1.70E-03
Long term potentiation (KEGG)	71	60	5	9.64E-15	2.97E-06
MAPK signaling pathway (KEGG)	268	233	5	3.02E-15	4.92E-03
HIV infection (Reactome)	208	163	5	1.32E-06	8.12E-04
HIV life cycle (Reactome)	126	95	5	1.03E-02	4.27E-05
Late phase of HIV life cycle (Reactome)	105	85	5	1.36E-02	2.27E-05
Neuronal system (Reactome)	280	219	5	3.80E-28	3.64E-03
NGF signalling via TRKa from the plasma membrane (Reactome)	138	120	5	1.09E-14	1.57E-04
Signaling by GPCR (Reactome)	921	415	5	1.63E-11	6.21E-02

doi:10.1371/journal.pgen.1006121.t002

As several tissues are enriched for subnetwork expression, we sought to understand whether we were capturing the same signature across multiple tissues reflecting a shared process. We assessed whether the same genes are preferentially expressed in each tissue, and found a distinct signature in the fetal brain and heart samples and the immune cell subpopulations ($CD34^+$, $CD8^+$, $CD3^+$, thymus; pairwise $p < 0.05$ hypergeometric test; S2 Table). To ensure our tissue expression results are not an artifact of the threshold we set for preferential expression, we repeated the entire analysis with a range of threshold values and found consistent results across tissues; this is most notable in fetal brain (Fig 2D and S3 Table), which remains significant irrespective of threshold used.

Genes under selective constraint are more likely to harbor pathogenic mutations causing Mendelian diseases, consistent with intolerance of functional mutations [6]. Accordingly, we found that our subnetwork of 72 genes is significantly enriched for OMIM annotations (Fisher's exact $p = 0.0013$). To further elucidate this observation, we mapped all OMIM entries to Medical Subject Headings (MeSH) disease categories and assessed enrichment per organ system category. We found that our subnetwork is significantly enriched for genes mutated in Mendelian diseases affecting the central nervous system (Fisher's exact $p = 0.0017$, S5 Table), validating our observation of enrichment in fetal brain. We note that this enrichment is not in the inflammatory/immune neurological disease sub-category, suggesting no overlap with the discrete immune signature we found. Samocha *et al* [6] have previously reported that

Table 3. The 72-member constrained gene subnetwork is preferentially expressed in a range of tissues and brain structures. We find strong enrichment in a variety of tissues, predominantly neural and immune-derived samples sourced from the Roadmap Epigenome Project (REP) and the BrainSpan Atlas. We report only tissues passing significance with two conservative independent empirical approaches: random permutation of preferential expression values for the subnetwork across tissues (permutation); and comparison to the largest subnetworks detected when we permute constraint scores for all 9729 InWeb genes.

Source	Tissue	Developmental stage	Permutation p-value	Resampled p-value	Tissue-specific genes
REP	$CD34^+$	Perinatal (cord blood)	0.00100	0.00100	10
REP	Fetal brain	Fetal	0.01100	0.00100	16
REP	$CD8^+$	Adult (>20 years)	0.01700	0.00100	10
REP	Fetal thymus	Fetal	0.04800	0.00100	5
BrainSpan	Caudal ganglionic eminence	2A (8–9 pcw)	0.00125	0.00125	20
BrainSpan	Dorsolateral prefrontal cortex	2A (8–9 pcw)	0.00125	0.00125	16
BrainSpan	Hippocampal anlage	2A (8–9 pcw)	0.00125	0.00125	17
BrainSpan	Lateral ganglionic eminence	2A (8–9 pcw)	0.00125	0.00125	19
BrainSpan	Primary motor-sensory cortex	2A (8–9 pcw)	0.00125	0.00125	20
BrainSpan	Medial frontal cortex	2A (8–9 pcw)	0.00125	0.00125	19
BrainSpan	Orbital frontal cortex	2A (8–9 pcw)	0.00250	0.00125	14
BrainSpan	Parietal neocortex	2A (8–9 pcw)	0.00250	0.00125	18
BrainSpan	Medial ganglionic eminence	2A (8–9 pcw)	0.00375	0.00125	18
BrainSpan	Occipital neocortex	2A (8–9 pcw)	0.00500	0.00125	18
BrainSpan	Hippocampus	2B (10–12 pcw)	0.00625	0.00125	18
BrainSpan	Hippocampus	3A (13–15 pcw)	0.00625	0.00125	19
BrainSpan	Primary somatosensory cortex	3A (13–15 pcw)	0.01250	0.00125	20
BrainSpan	Primary visual cortex	4 (19–24 pcw)	0.01750	0.00125	22
BrainSpan	Posterior superior temporal cortex	3B (16–18 pcw)	0.01875	0.00125	22
BrainSpan	Posteroventral parietal cortex	3A (13–15 pcw)	0.02250	0.00125	19
BrainSpan	Cerebellar cortex	4 (19–24 pcw)	0.02500	0.00125	19
BrainSpan	Primary motor cortex	3A (13–15 pcw)	0.02750	0.00125	19
BrainSpan	Striatum	3A (13–15 pcw)	0.04125	0.00125	17
BrainSpan	Dorsolateral prefrontal cortex	4A (19–24 pcw)	0.04625	0.00250	21

doi:10.1371/journal.pgen.1006121.t003

constrained genes are also enriched for *de novo* mutations associated with autism spectrum disorders, further strengthening our conclusion that this constrained subnetwork represents a brain-related biological process.

The constrained module is preferentially expressed in early brain development

To further elucidate the relevance of our constrained module to brain physiology, we interrogated expression data for multiple brain structures across developmental stages from the BrainSpan project [15]. We found a strong signature of preferential expression in very early stages of development, which declines rapidly and is absent by mid-gestation and remains inactive after birth into adulthood (Fig 3A and Table 3). Several transitional structures in the early brain exhibit significant preferential expression levels, including the ganglionic eminences that eventually form the ventral forebrain and the early structures of the hippocampus. The latter structure shows the most consistent signature across developmental time, with the module's pattern of expression gradually weakening and becoming non-significant by mid gestation (post-conception weeks 16–18; Fig 3B). These results, taken with the likely involvement of constrained genes in fundamental processes of mitosis and transcriptional regulation,

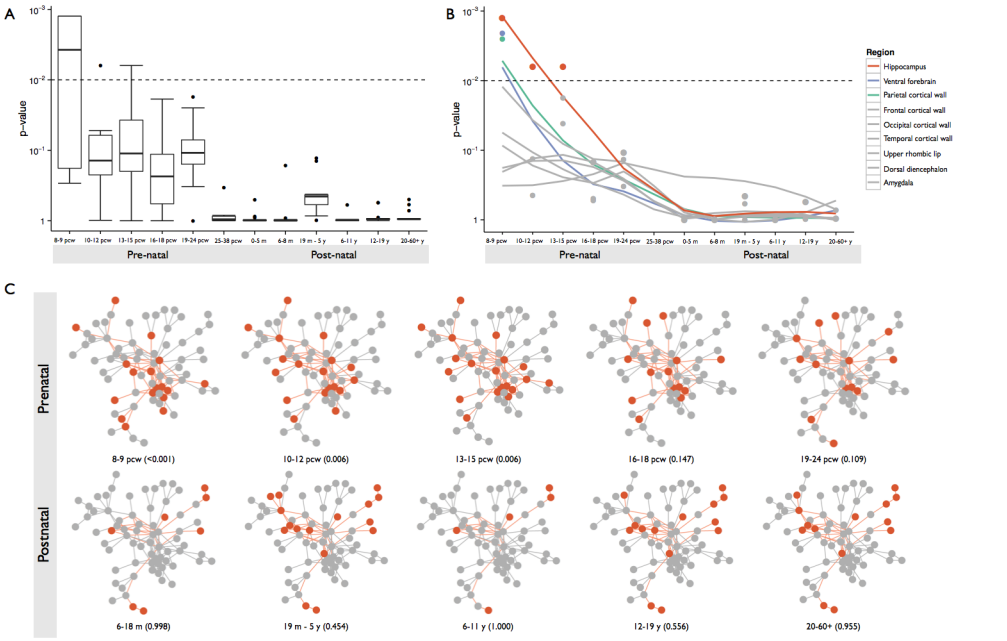

Fig 3. the 72-member selectively constrained gene subnetwork is active in early brain development, particularly in the hippocampus. A: the constrained subnetwork shows elevated signatures of preferential expression in early stages of brain development. B: the signature is most robust in the hippocampus and its ancestral structures (orange), with some enrichment in ventral forebrain and parietal cortical wall structures very early in development (8–9 post-conception weeks). C: The constrained subnetwork shows significant preferential expression in early developmental stages, with patterns of expression losing this enrichment signature by mid-gestation. Preferentially expressed nodes and the shortest paths connecting them are colored orange; grey nodes are not preferentially expressed in each displayed tissue. Overall, these data suggest the constrained subnetwork is specifically active in very early stages of hippocampal formation.

doi:10.1371/journal.pgen.1006121.g003

suggest this gene module is relevant to developmental patterning at crucial time points in early brain development.

Discussion

We have shown that selective constraint influences sets of interacting genes involved in core cellular control processes, and that these have elevated expression levels in early stages of central nervous system development. We found the strongest enrichment in the early hippocampal stages at post-conception weeks eight and nine, with additional signals in ventral forebrain structures and the parietal cortical wall. This stage of development involves neuronal proliferation through carefully orchestrated sequences of cell differentiation during developmental patterning across the brain. As the constrained subnetwork we have detected is enriched for genes involved in the control of mitosis and transcription, we speculate that it plays a fundamental role in these processes. Our finding that neurological Mendelian disease genes are over-represented, combined with previous reports of *de novo* mutations affecting autism spectrum disorders [6,18], intellectual disability [6] and epileptic encephalopathy [5], further support this notion, indicating that most perturbation leads to severe phenotype. This strong limitation in tolerance may also explain our observation of enrichment in immune cell populations, as precise control of developmental decisions is crucial to the correct differentiation of the lymphoid and myeloid lineages throughout life. As the selective constraint scores are by design corrected for both coding sequence length and GC bias [6], constraint is more likely to be due to

intolerance of changes to protein function rather than structural characteristics of the encoded proteins.

Network analyses have been used to identify interacting groups of genes conserved across species [19], and to identify groups of co-expressed genes in both healthy individuals [20] and groups of genes whose expression is coordinately altered in neurological disease [21]. In particular, network analyses of expression data across species suggest that co-regulated genes form stable interaction networks that evolve in a coordinate fashion [19]. These diverse analyses all suggest that functionally linked genes form stable networks and are targets of natural selection due to their group contribution to specific biological processes [22]. Our own results support this notion, demonstrating that interacting protein networks are under remarkable constraint within the human species, presumably because they underlie carefully orchestrated biological processes.

More broadly, our results present a glimpse into how natural selection may affect entire groups of genes involved in central homeostatic functions. Most studies of selection aim to identify specific alleles inconsistent with the nearly neutral model of drift, with particular success in studies of recent positive selection [23,24]. We suggest that the majority of these effects represent near-Mendelian effects on relevant phenotypes, which are the actual targets of selective forces: for example, variability in lactase persistence is almost entirely explained by any one of handful of necessary and sufficient alleles [25]. However, the majority of human traits are polygenic, and selection would likely exert far weaker effects on risk alleles, most of which have been revealed by GWAS to only explain a fraction of phenotypic variance. Although such polygenic adaptation [26] has proven difficult to detect thus far, our data provide confirmation that selective forces can act on groups of genes involved in the same process, supporting the notion that purifying selection can act coordinately on multiple genes. We describe how selective constraint acts on groups of genes, suggesting such coordination, though we note that the constraint statistics contain no information about whether multiple genes are targets of the same pressure. We further note that the substantial preferential expression we see does not apply to the entire constrained subnetwork—this may be due either to imprecise specification of the network itself or limitations in detecting preferential expression in a limited tissue atlas. However, our results clearly support a coherent physiological role for this network in early fetal development.

We have presented a robust approach to identifying sets of interacting genes under selective constraint and placing these into biological context, using the wealth of genome-scale data produced by large-scale public projects. Our approach builds on robust statistical frameworks to interrogate single variants or genes and thus provides previously lacking biological context from which further hypotheses can be drawn. The approach is flexible and not restricted to studies of constraint: per-gene measures derived from studies of other forms of natural selection, non-human hominid introgression, common and rare variant disease association can be analyzed in our framework. Further, as PINTS is modular, appropriate tissue atlases can be used to meaningfully interpret results. We believe our work represents a new class of approaches that can leverage multiple genome-scale datasets to gain new insight into biological activities responsible for health and disease.

Materials and Methods

Selective constraint data

We have used selective constraint scores as previously described [6]. Briefly, we used a mutation rate table—containing the probability of every trinucleotide XY_1Z mutating to every other possible trinucleotide XY_2Z—based on intergenic SNPs from the 1000 Genomes project and

the sequence of a gene to determine that gene's probability of mutation. These sequence context-based probabilities of mutation were additionally corrected for regional divergence between humans and macaques as well as the depth of coverage for each base in an exome sequencing study. Given the high correlation (Pearson's r = 0.94) between the probability of a synonymous mutation in a gene with the number of rare (MAF < 0.01%) synonymous variants in that gene seen in the NHLBI's Exome Sequencing Project, we used a linear model to predict the number of rare missense variants expected per gene in the same dataset. The difference between observation and expectation was quantified as a signed Z score of the chi-squared deviation. The missense Z score was used as the basis for determining selective constraint. In this study, we took a conservative approach to assessing selective constraint, using the Bonferroni correction for number of InWeb genes to derive a significance threshold of $p_c < 5 \times 10^{-6}$.

Detecting selectively constrained subnetworks in protein-protein interaction data

We used InWeb, a previously described comprehensive map of protein-protein interactions, containing 169,736 high-confidence interactions between 12,687 gene products, compiled from a variety of sources [16]. By mapping ENSEMBL IDs, we were able to identify 9729 genes with constraint scores from Samocha *et al* [6] also present in the REP expression data (below), to which we restricted our analysis.

To detect clusters of interacting constrained genes, we used a heuristic form of the prize-collecting Steiner tree (PCST) algorithm [27,28], which has been previously applied to protein-protein interaction data[17]. The canonical form of the PCST algorithm takes a connected, undirected graph $G(V,E,w,u)$ with V vertices and E edges, with vertex weights w and edge weights u; it then finds the connected subgraph $T(V',E')$ with maximal $profit(T)$, which is some function of $(w'-u')$. By definition, T is a minimal spanning tree. The algorithm thus identifies the set of nodes with the strongest signal given the *cost* of their connecting edges. The classical PCST algorithm is, however, *NP-hard*, which makes it computationally intractable on the scale of InWeb [27]. Several heuristic simplifications have been proposed, including one previously validated as suitable for protein-protein interaction networks which we use here [17]. This approach partitions the set V into *null* (with weights $w < 0$) and *signal* (with weights $w > 0$) vertices (genes) and equal edge weights e before searching for T. Beisser *et al* have implemented this approach in the BioNet package for the R statistical language [29]. Here, we define signal genes as those with constraint scores passing the Bonferroni threshold of $p_c < 5 \times 10^{-6}$, and calculate the weights as $w = -log(p_c) + log(5 \times 10^{-6})$. The PCST algorithm returns a single, maximal T solution; to discover further independent subnetworks, we apply the method iteratively after we assign gene nodes in the previously discovered solution to be null.

The algorithm always returns a solution for T, so we sought to assess the significance of our observations empirically. To understand if the observed solution is unlikely by chance, we permuted the constraint scores of genes 1000 times and for each iteration ran the heuristic PCST to generate 1000 random *resampled subnetworks* (these are also used in the tissue-specificity analyses described below). We then quantified the following key parameters and assessed how many random subnetworks had values exceeding those of the true discovered subnetwork: size (number of gene nodes); density (number of connections); clustering coefficient and total amount of constraint explained (sum of constraint scores). To address the possible contribution of degree bias to these results, we also performed biased permutations to select signal nodes with the same degree distribution as we had previously done for DAPPLE [9]. We found weak correlation between degree and significance (S1 Fig) and opted for random permutations where the number of combinations of random genes selected as signal nodes is much larger.

Gene expression data processing and preferential expression analysis

We obtained gene expression data for a cosmopolitan set of tissues from the Roadmap Epigenome Project (REP) [14]. The REP data consists of 88 samples across 27 tissue types from diverse human organs, profiled on the Affymetrix HuEx-1_0-st-v2 exon array, which we downloaded on 9/25/2013 from http://www.genboree.org/EdaccData/Current-Release/experiment-sample/Expression_Array/. We processed these data using standard methods available from the BioConductor project [30,31]. Briefly, we removed cross-hybridizing probesets, applied RMA background correction and quantile normalization and then summarized probesets to transcript-level intensities. We then mapped transcripts to genes using the current Gencode annotations for human genes (version 12). Transcripts with no match in Gencode were removed and the remaining transcripts we again quantile normalized. We then assigned transcript expression levels to their matching genes. Where multiple transcripts mapped to the same gene we used the transcript with maximum expression over all cell types.

The Brainspan atlas [15] data are available as processed, gene-level expression levels from http://www.brainspan.org/static/download.html. We mapped these genes to the InWeb gene set using ENSEMBL IDs, and quantile normalized data for the overlapping genes. We then grouped replicate data by developmental stage and brain structure and calculated preferential expression as described above.

We used a previously described approach to detect tissue-specific expression across each tissue atlas [32]. Briefly, we group together replicates from the same cell type and compute pairwise differential expression between all pairwise combinations of tissues, using an empirical Bayes approach to account for variance shrinkage [33]. Thus, for each gene there are 26 linear model coefficients and associated p values for each tissue, quantifying the comparison to all other tissues. For each gene in each tissue, we then capture the overall difference in expression from all other tissues as the sum of these coefficients. To reduce noise, only coefficients with $p < 0.0019$ ($p < 0.05$ with Bonferroni correction for 26 tissues) are considered. Rescaling all coefficient sums across all genes values to the range [−1,1] gives us a final preferential expression score. Intuitively, a gene highly expressed in only one tissue would get a high positive enrichment score in that tissue, as it is differentially expressed compared to all other tissues. The score is directional, strong negative values indicate very low expression in one tissue compared to all others. We partition the overall distribution into deciles and define preferential expression in a tissue if a gene has a score > 0.1.

Scoring subnetwork tissue specificity

To score the tissue specific expression of a subnetwork, we detect which genes in the subnetwork are preferentially expressed in each tissue of our expression atlas and assess the joint probability of this observation. Rather than ask if some nodes of the subnetwork are preferentially expressed in a given tissue, we developed an approach to account for the connections between genes; we thus assess whether the pattern of preferential expression across the whole subnetwork is unusual for a given tissue, suggesting the subnetwork is operational. Formally, we consider the subnetwork as a Markov random field with a particular configuration of preferentially expressed nodes in each atlas tissue. We compute a score for each configuration using a standard scoring function [34]:

$$P(x_1, \ldots, x_n) = \frac{1}{Z} \prod_{(i,j) \in Edges} \Phi(x_i, x_j)$$

The partition function Z is defined as:

$$Z = \sum_{x_1,\ldots,x_n} \prod_{(i,j)\in Edges} \Phi(x_i,\ x_j)$$

where $x_i (i = 1, \ldots, n)$represents a binary tissue specificity of the genes in the subnetwork for a given tissue with values either 1 (expressed) or 0 (not expressed). The $\Phi(x_i,x_j)$ factor lists the co-occurrence of two connected nodes across tissues. This is calculated from the thresholded preferential expression data, and each pair of connected nodes is assigned exactly one *configuration* in each tissue, so that

$$\Phi(x_i = 0,\ x_j = 0) + \Phi(x_i = 1,\ x_j = 0) + \ \Phi(x_i = 0,\ x_j = 1) + \ \Phi(x_i = 1,\ x_j = 1) = number\ of\ tissues$$

We assess the significance of these scores using two conservative permutation approaches. First we assess how likely we are to see each observed configuration (i.e. each pattern of detected/not detected nodes) in each tissue of the atlas. We do this by permuting the preferential expression scores across tissues for each gene independently and rescoring the configuration found in each tissue. This alters the co-expression structure across genes and empirically assesses how likely we are to see a particular configuration of a specific subnetwork by chance. Second, we estimate the probability of observing the extent of tissue specificity in each tissue. We construct the null expectation by scoring the *resampled subnetworks* generated by permutation above in each tissue and compute the empirical significance from this distribution of scores.

To ensure our results are not artifacts of a specific preferential expression threshold, we repeat this analysis across a spectrum of preferential expression thresholds (See S3 Table).

Pathway analysis

To test if any biological pathways are over represented in a subnetwork, we use the Gene Set Enrichment Analysis (GSEA) approach [35]. We obtained the full list of curated canonical pathways from the GSEA website (http://www.broadinstitute.org/gsea/msigdb/collections.jsp) and mapped the 9729 genes to each pathway using HUGO IDs. We then test for enrichment of subnetwork members over background using the hypergeometric test.

Online Mendelian Inheritance in Man (OMIM) analysis

To test if genes in the subnetwork are more likely to harbor pathogenic mutations causing Mendelian diseases than expected by chance, we retrieved OMIM records for all 9729 genes using the biomaRt package in BioConductor [31]. We then tested whether the proportion of 107 subnetwork genes with OMIM entries was higher than the background proportion of the full set of 9729 in our analysis using Fisher's exact test (S4 Table). We then mapped all OMIM entries to Medical Subject Headings (MeSH) disease categories using the Comparative Toxicogenomics Database (CTD) MEDIC disease vocabulary [36] and assessed enrichment in any disease category, again using Fisher's exact test (S6 Table).

Supporting Information

S1 Table. Significance of the clustering of the top subnetwork in InWeb PPI network. The mutational constraint signals (genes) in the top subnetwork show the significance clustering in terms of the number of nodes and edges and the clustering coefficient, and the constraint score

sum against null expectation suggesting they function together.
(PDF)

S2 Table. Threshold dependence analysis of significant tissues associated with mutational constraint gene network using Roadmap epigenomics dataset. Shown in the table are the p values of all significant tissues at a nominal significance (p = 0.05). Fetal brain shows consistently strong signal across all the threshold values. It suggests that fetal brain is most likely tissue of action.
(PDF)

S3 Table. Threshold dependence of tissue specific gene count summary. Shown in the table includes: i) the number of tissue specific genes in the top subnetwork across the threseholds for all significant tissues. ii) the average number of tissue specific genes in the top subnetwork as well as entire network. iii) The median and standard deviation of tissue specific genes per tissues. iv) the mean and the standard deviation of tissue specificity of all genes.
(PDF)

S4 Table. Tissue specific gene overlap among significant tissues. We do not see significant overlap between the 72 genes in our constrained network that are preferentially expressed in fetal brain with those preferentially expressed in immune-system related cell types. This suggests that the tissue specific action of fetal brain is independent from that of immune-system related cell/tissue types.
(PDF)

S5 Table. Online in Man in Mendelian (OMIM) record enrichment analysis of gene sets. All genes in top subnetwork, tissue-specific genes in the significant tissues such as fetal brain/CD34/CD8/fetal thymus, and all genome-wide significant mutational constraint genes. The total counts indicate the number of genes identified to have OMIM entries through biomarRt R package. The numbers in parenthesis indicate the actual total number of gene sets.
(PDF)

S6 Table. Medical Subject Headings (MeSH) disease category enrichment analysis for all genes in the top subnetwork. Among all the disease categories mapped to by at least one gene, only the nervous system disease shows significance.
(PDF)

S7 Table. Pathway enrichment analysis using canonical curated pathways. Each column represents the following: Column 1: Curated pathway name; Column 2: Number of genes in each pathway; Column 3: Number of genes that are mapped to InWeb PPI network; Column 4: Number of genes in top subnetwork; Column 5: p-value of Gene Set Enrichment Analysis (Kolmogrov-Smirnov test); Column 6: p-value of hypergeometric test
(PDF)

S8 Table. Binary tissue specificity of all genes in the top subnetwork for a subset of significant tissues among all tissues in Roadmap and BrainSpan gene expression dataset.
(PDF)

S1 Fig. Correlation between InWEB node degree and constraint scores. Constraint Z scores are only weakly correlated with InWEB node degree. Pearson correlation coefficient = 0.022.
(PDF)

S1 Text. Supplementary methods.
(PDF)

Acknowledgments

We acknowledge our use of the gene set enrichment analysis, GSEA software, and Molecular Signature Database (MSigDB), available at http://www.broad.mit.edu/gsea/.

Author Contributions

Conceived and designed the experiments: JC PS CC. Performed the experiments: JC PS. Analyzed the data: JC PS CC. Contributed reagents/materials/analysis tools: KES MJD. Wrote the paper: JC PS CC.

References

1. Nielsen R, Hellmann I, Hubisz M, Bustamante C, Clark AG. Recent and ongoing selection in the human genome. Nature Reviews Genetics. 2007; 8: 857–868. doi: 10.1038/nrg2187 PMID: 17943193
2. Ng SB, Bigham AW, Buckingham KJ, Hannibal MC, McMillin MJ, Gildersleeve HI, et al. Exome sequencing identifies MLL2 mutations as a cause of Kabuki syndrome. Nature Genetics. Nature Publishing Group; 2010; 42: 790–793. doi: 10.1038/ng.646
3. Sanders SJ, He X, Willsey AJ, Ercan-Sencicek AG, Samocha KE, Cicek AE, et al. Insights into Autism Spectrum Disorder Genomic Architecture and Biology from 71 Risk Loci. Neuron. Elsevier; 2015; 87: 1215–1233. doi: 10.1016/j.neuron.2015.09.016
4. Robinson EB, St Pourcain B, Anttila V, Kosmicki JA, Bulik-Sullivan B, Grove J, et al. Genetic risk for autism spectrum disorders and neuropsychiatric variation in the general population. Nature Genetics. 2016; 48: 552–555. doi: 10.1038/ng.3529 PMID: 26998691
5. Epi4K Consortium, Epilepsy Phenome/Genome Project, Allen AS, Cossette P, Delanty N, Eichler EE, et al. De novo mutations in epileptic encephalopathies. Nature. 2013; 501: 217–221. doi: 10.1038/nature12439 PMID: 23934111
6. Samocha KE, Robinson EB, Sanders SJ, Stevens C, Sabo A, McGrath LM, et al. A framework for the interpretation of de novo mutation in human disease. Nature Genetics. 2014; 46: 944–950. doi: 10.1038/ng.3050 PMID: 25086666
7. Yang J, Manolio TA, Pasquale LR, Boerwinkle E, Caporaso N, Cunningham JM, et al. Genome partitioning of genetic variation for complex traits using common SNPs. Nature Genetics. 2011; 43: 519–525. doi: 10.1038/ng.823 PMID: 21552263
8. Yang J, Benyamin B, McEvoy BP, Gordon S, Henders AK, Nyholt DR, et al. Common SNPs explain a large proportion of the heritability for human height. Nature Genetics. 2010; 42: 565–569. doi: 10.1038/ng.608 PMID: 20562875
9. Rossin EJ, Lage K, Raychaudhuri S, Xavier RJ, Tatar D, Benita Y, et al. Proteins encoded in genomic regions associated with immune-mediated disease physically interact and suggest underlying biology. PLoS Genetics. 2011; 7: e1001273. doi: 10.1371/journal.pgen.1001273 PMID: 21249183
10. Hormozdiari F, Kichaev G, Yang W-Y, Pasaniuc B, Eskin E. Identification of causal genes for complex traits. Bioinformatics. Oxford University Press; 2015; 31: i206–i213. doi: 10.1093/bioinformatics/btv240
11. Lee Y, Li H, Li J, Rebman E, Achour I, Regan KE, et al. Network models of genome-wide association studies uncover the topological centrality of protein interactions in complex diseases. Journal of the American Medical Informatics Association. 2013. doi: 10.1136/amiajnl-2012-001519
12. Hormozdiari F, Penn O, Borenstein E, Eichler EE. The discovery of integrated gene networks for autism and related disorders. Genome Research. Cold Spring Harbor Lab; 2015; 25: 142–154. doi: 10.1101/gr.178855.114
13. Maurano MT, Humbert R, Rynes E, Thurman RE, Haugen E, Wang H, et al. Systematic Localization of Common Disease-Associated Variation in Regulatory DNA. Science. 2012; 337: 1190–1195. doi: 10.1126/science.1222794 PMID: 22955828
14. Bernstein BE, Stamatoyannopoulos JA, Costello JF, Ren B, Milosavljevic A, Meissner A, et al. The NIH Roadmap Epigenomics Mapping Consortium. Nat Biotechnol. Nature Publishing Group; 2010; 28: 1045–1048. doi: 10.1038/nbt1010-1045
15. Kang HJ, Kawasawa YI, Cheng F, Zhu Y, Xu X, Li M, et al. Spatio-temporal transcriptome of the human brain. Nature. Nature Publishing Group; 2011; 478: 483–489. doi: 10.1038/nature10523
16. Lage K, Karlberg EO, Størling ZM, Ólason PÍ, Pedersen AG, Rigina O, et al. A human phenome-interactome network of protein complexes implicated in genetic disorders. Nat Biotechnol. 2007; 25: 309–316. doi: 10.1038/nbt1295 PMID: 17344885

17. Dittrich MT, Klau GW, Rosenwald A, Dandekar T, Muller T. Identifying functional modules in protein-protein interaction networks: an integrated exact approach. Bioinformatics. 2008; 24: i223–i231. doi: 10.1093/bioinformatics/btn161 PMID: 18586718

18. Neale BM, Kou Y, Liu L, Ma'ayan A, Samocha KE, Sabo A, et al. Patterns and rates of exonic de novo mutations in autism spectrum disorders. Nature. 2012; 485: 242–245. doi: 10.1038/nature11011 PMID: 22495311

19. Oldham MC, Horvath S, Geschwind DH. Conservation and evolution of gene coexpression networks in human and chimpanzee brains. Proceedings of the National Academy of Sciences. National Acad Sciences; 2006; 103: 17973–17978. doi: 10.1073/pnas.0605938103

20. Kircher M, He Z, Guo S, Fairbrother GL. Evaluating intra-and inter-individual variation in the human placental transcriptome. Genome . . .. 2015.

21. Voineagu I, Wang X, Johnston P, Lowe JK, Tian Y, Horvath S, et al. Transcriptomic analysis of autistic brain reveals convergent molecular pathology. Nature. Nature Publishing Group; 2011;: 1–7. doi: 10.1038/nature10110

22. Wagner GP, Zhang J. The pleiotropic structure of the genotype–phenotype map: the evolvability of complex organisms. Nature Reviews Genetics. Nature Publishing Group; 2011; 12: 204–213. doi: 10.1038/nrg2949

23. Grossman SR, Shlyakhter I, Shylakhter I, Karlsson EK, Byrne EH, Morales S, et al. A composite of multiple signals distinguishes causal variants in regions of positive selection. Science. American Association for the Advancement of Science; 2010; 327: 883–886. doi: 10.1126/science.1183863

24. Sabeti PC, Fry B, Lohmueller J, Hostetter E, Cotsapas C, Xie X, et al. Genome-wide detection and characterization of positive selection in human populations. Nature. 2007; 449: 913–918. doi: 10.1038/nature06250 PMID: 17943131

25. Scheinfeldt LB, Tishkoff SA. Recent human adaptation: genomic approaches, interpretation and insights. Nature Reviews Genetics. 2013; 14: 692–702. doi: 10.1038/nrg3604 PMID: 24052086

26. Pritchard JK, Di Rienzo A. Adaptation—not by sweeps alone. Nature Reviews Genetics. Nature Publishing Group; 2010; 11: 665–667. doi: 10.1038/nrg2880

27. Ljubić I, Weiskircher R, Pferschy U, Klau GW, Mutzel P, Fischetti M. An Algorithmic Framework for the Exact Solution of the Prize-Collecting Steiner Tree Problem. Math Program. Springer-Verlag; 2006; 105: 427–449. doi: 10.1007/s10107-005-0660-x

28. Ljubic I, Weiskircher R, Pferschy U, Klau GW. Solving the prize-collecting Steiner tree problem to optimality. ALENEX/ANALCO. 2005.

29. Beisser D, Klau GW, Dandekar T, Müller T, Dittrich MT. BioNet: an R-Package for the functional analysis of biological networks. Bioinformatics. Oxford University Press; 2010; 26: 1129–1130. doi: 10.1093/bioinformatics/btq089

30. Gautier L, Cope L, Bolstad BM, Irizarry RA. affy—analysis of Affymetrix GeneChip data at the probe level. Bioinformatics. Oxford University Press; 2004; 20: 307–315. doi: 10.1093/bioinformatics/btg405

31. Gentleman RC, Carey VJ, Bates DM, Ben Bolstad, Dettling M, Dudoit S, et al. Bioconductor: open software development for computational biology and bioinformatics. Genome Biol. BioMed Central Ltd; 2004; 5: R80. doi: 10.1186/gb-2004-5-10-r80

32. Benita Y, Cao Z, Giallourakis C, Li C, Gardet A, Xavier RJ. Gene enrichment profiles reveal T-cell development, differentiation, and lineage-specific transcription factors including ZBTB25 as a novel NF-AT repressor. Blood. 2010; 115: 5376–5384. doi: 10.1182/blood-2010-01-263855 PMID: 20410506

33. Smyth GK. limma: Linear Models for Microarray Data. Bioinformatics and Computational Biology Solutions Using R and Bioconductor. New York: Springer New York; 2005. pp. 397–420. doi: 10.1007/0-387-29362-0_23

34. Schmidt M. UGM: Matlab code for undirected graphical models [Internet]. Vancouver, Canada; [cited 28 Mar 2015]. Available: http://www.cs.ubc.ca/~schmidtm/Software/UGM.html

35. Subramanian A, Tamayo P, Mootha VK, Mukherjee S, Ebert BL, Gillette MA, et al. Gene set enrichment analysis: a knowledge-based approach for interpreting genome-wide expression profiles. Proc Natl Acad Sci USA. National Acad Sciences; 2005; 102: 15545–15550. doi: 10.1073/pnas.0506580102

36. Davis AP, Grondin CJ, Lennon-Hopkins K, Saraceni-Richards C, Sciaky D, King BL, et al. The Comparative Toxicogenomics Database's 10th year anniversary: update 2015. Nucleic Acids Research. Oxford University Press; 2015; 43: D914–20. doi: 10.1093/nar/gku935